RSC Applied Polymers

ROYAL SOCIETY OF CHEMISTRY

PAPER

View Article Online
View Journal

Cite this: DOI: 10.1039/d6lp00034g

Standalone 3-D piezoelectric polymer–ceramic foam for efficient energy harvesting

Alekhika Tripathy,†[a] Jyoti Prakash Das, †[b] Balasubramaniam Saravanakumar,[a] Sang Jae Kim [b] and Ananthakumar Ramadoss *†[c]

Received 30th January 2026,
Accepted 3rd May 2026

DOI: 10.1039/d6lp00034g

rsc.li/rscapplpolym

The rising demand for wearable electronics has drawn widespread attention to piezoelectric materials due to their potential application in low-power devices. Herein, a unique method is adopted for fabricating free-standing foam-structured piezoelectric nanogenerators (PENGs) with excellent piezoelectric response using polyvinylidene fluoride (PVDF) embedded with piezoceramics. The as-fabricated foam with a porous structure and good flexibility delivered a maximum piezoelectric output voltage and current of 11.61 V and 70 nA. Both PVDF and the integrated ceramic nanoparticles in the composite foams contribute to the piezoelectric performance, thus giving better output compared to the pristine PVDF foam. Moreover, the interconnected pores within the foam structure provide a high surface area endowing the material with good amount of stress concentration sites that help in improving the piezoelectric voltage, respectively. This work presents a convenient method for designing mechanical energy harvesters that have great potential in self-powered wearable electronic devices.

1 Introduction

Mechanically flexible piezoelectric materials are in considerable demand for use in energy-scavenging devices.[1–8] However, these two characteristics, piezoelectricity and mechanical flexibility, are incompatible since they cannot be enhanced simultaneously. Although polymers like PVDF possess mechanical flexibility and ease of processing, their piezoelectric coefficients are substantially lower than those of piezoelectric ceramics.[9–14] The latter, with high piezoelectric coefficients, cannot be fabricated in mechanically compliant structures because mechanical strain rapidly fractures them. So, in order to produce mechanically flexible structures, several topologies such as thin films and nanowire arrays using piezoelectric ceramics and semiconductor oxides have been investigated recently. The processing techniques of these one-dimensional (1D) and two-dimensional (2D) nanostructures not only pose constraints for large-scale production but are also cost-intensive. Another demerit of these lower dimensional structures is that they have limited loading directions that are responsible for the piezoelectric effect. Henceforth, constructing higher-order structures with substantial mechanical flexibility is critical for applications such as acoustic transducers, wearable electronic devices, compact energy harvesters, and so on.

Most of the traditional PENGs are 2D structures which fail to amplify the piezoelectric output. The primary reason behind this is that the 2D structures do not consider normal strains but only the transverse and longitudinal strains,[15,16] whereas in a 3D structure, the total space contributes towards generating the larger piezoelectric strain.[17] Therefore, many research studies have been carried out on 3D energy harvesters as listed in the comparison table in a later section. These studies clearly show that compared to planar structures, the piezoelectric output voltage of 3D structures is many times higher. In particular, unlike bulk materials, materials with a porous structure have smaller volumes and lower moduli, and hence acquire larger compression strain thereby generating higher piezoelectric output.[18–20] Generally, porous structures are more flexible compared to bulk materials. Due to this, applying a similar force can generate larger strain and voltage output in a porous material than in a bulk one.[21] Beyond offering flexibility, the enhanced piezoelectric performance of these foamed porous structures arises from a synergistic interaction between the material's components and its architecture. In particular, the large surface area of interconnected pores serves as stress concentration sites, intensifying localized deformation, thereby maximizing the piezoelectric energy output.[22]

[a]School for Advanced Research in Polymers: Laboratory for Advanced Research in Polymeric Materials (LARPM), Central Institute of Petrochemicals Engineering and Technology (CIPET), Bhubaneswar-751024, India
[b]Nanomaterials and Systems Lab, Major in Mechatronics Engineering, Faculty of Applied Energy System, Jeju National University, Jeju, 63243, South Korea
[c]School for Advanced Research in Polymers: Advanced Research School for Technology & Product Simulation, Central Institute of Petrochemicals Engineering & Technology, Guindy, Chennai – 600032, India. E-mail: ananth.cipet@gmail.com, ananth@cipet.gov.in
†These authors contributed equally.

In the case of piezoelectric ceramics, the relative permittivity decreases with increasing porosity. This can be attributed to the simultaneous increase in surface area and space-charge fields based on the space-charge theory.[23] To date, many research studies have been conducted to introduce porosity into dense materials in order to reduce the permittivity of sensor materials.[24–27] Piezoelectric sensitivity might increase in devices with better piezoelectric symmetry, which could lead to a variety of fascinating applications. Foams are such structures, which are made up of materials packed in a random network with a higher void proportion. Conventionally, piezoceramics are used in developing such piezoelectric materials *via* robocasting[28] or fused-deposition[29] techniques to prepare porous structures layer-by-layer or by polymer templating. Lead zirconate titanate (PZT)-based foams have been discovered to have lower acoustic impedance, greater mechanical flexibility, and higher piezo-sensitivity than other thin films, and have thus been employed in a variety of applications such as actuators, wide-band hydrophones, and so on.[30,31] Even though the porous structure improves the mechanical and electrical capabilities of the piezoceramics, they remain fragile.

For this purpose, piezoelectric polymers are widely being integrated to maintain isotropic mechanical stability along with providing merits like higher elasticity, biocompatibility, easy processability, *etc*. In addition to their cost-effective synthesis methods they also offer good piezoelectric output. PVDF is a well-known piezoelectric material with a piezoelectric coefficient (d_{33}) ranging from 20 to 34 pC N^{-1}. Although its coefficient is considerably lower than that of piezoceramics, PVDF is commonly used in a wide range of applications because of its favorable mechanical and electrical properties. PVDF has been electrospun into fibres to improve its integration capability and flexibility, allowing it to be employed in applications such as hydrophones,[32] acoustic transmitters,[33] nonvolatile low-voltage memory,[34] implantable medical devices,[35] and so on. There are numerous reported studies involving the production of PVDF foams for efficient energy harvesters.[27,36] As a result, numerous piezoelectric composite foams exhibiting excellent flexibility and strong piezoelectric performance have been produced. These foam structures are obtained *via* different methods, such as sol–gel[37] by the addition of foaming additives,[38] or by the use of supercritical carbon dioxide,[39] *etc*.

This work reports achieving a highly porous foam structure that is exceedingly soft and flexible through a simple and scalable process. In order to simultaneously obtain a significant piezoelectric output and retain structural isotropy, this work presents the development of a highly elastic piezoelectric composite-based foam structure using PVDF and ceramics like $BiFeO_3$ (BFO) and K(Na, Nb)O_3 (KNN), providing a comprehensive evaluation of their piezoelectric performance. The composite foam was fabricated by molding a PVDF–piezoelectric nanoparticle (NP) dispersion within a sacrificial nickel (Ni) framework. Subsequent removal of the Ni template resulted in a well-interconnected foam structure with well-dispersed constituents.

2 Experimental section

2.1 Materials

The starting materials used in the synthesis of BFO and KNN include Bi $(NO_3)_2{\cdot}6H_2O$ (Sigma Aldrich Pvt. Ltd), Fe $(NO_3)_3{\cdot}9H_2O$ (Himedia Pvt. Ltd), Nitric acid (Himedia Pvt. Ltd), Nb_2O_5 (Himedia Pvt. Ltd), KOH (Himedia Pvt. Ltd) and NaOH (Himedia Pvt. Ltd). For foam fabrication, the materials used were PVDF powder (Sigma Aldrich, India), *N*,*N*-dimethyl formamide (DMF) procured from SRL Pvt. Ltd, India, and Nickel foam (Taiwan, 2 mm thickness, 95% porosity).

2.2 Preparation of PVDF-based piezoceramic composite foams *via* a template-assisted process

The PVDF-based composite foams were prepared as per the following procedure. The piezoceramics, such as BFO and KNN NPs, were synthesized *via* a hydrothermal process. The details of the procedure for the synthesis of piezoceramic NPs are given in the supporting information (SI). The optimized weight percentage (6 wt%) of PVDF was added to DMF solvent in a beaker and then stirred at 60 °C at 400 rpm for 3 h to ensure complete dispersion of the particles within the solution. After its complete dissolution in the solvent, piezoceramic NPs in the compositions of 2 and 4 wt% were added to the solution individually and stirring was continued for two hours. A Ni foam (5 cm × 3 cm) was taken and dipped in the prepared solution named as PVDF-2%-BFO, PVDF-4%-BFO, PVDF-2%-KNN and PVDF-4%-KNN at 60 °C in an oven. After the foam was completely dried, it was again dipped in the solution and then dried under the same conditions. This dipping and drying process was repeated multiple times to achieve compactness of the composite foam. The weight of the foam before and after the dip-coating was measured. Furthermore, to obtain a porous structured PVDF nanocomposite framework, Ni was etched out by immersing the foam in a concentrated HNO_3 solution (pH ~ 4), followed by rinsing the foam in DI water and drying at 60 °C. Then the weight of the foam was measured and it was found that >95% of Ni was removed. The average thickness of the foam samples was found to be 1.8 mm. The pristine PVDF foam was also fabricated by dipping a Ni foam in the first solution without the addition of ceramics, and then the same procedure was followed to obtain the pure PVDF foam. Finally, different types of 3D foam structures were obtained (PVDF and composite foams). The schematic of the preparation technique of the foam and its electrical measurement set-up is shown in Fig. 1a and b.

2.3 Fabrication and testing of the PENG device based on the PVDF-piezoceramic composite foam

A piezoelectric nanogenerator (PENG) was fabricated using the as-prepared piezoelectric foams (PVDF, PVDF-KNN, and

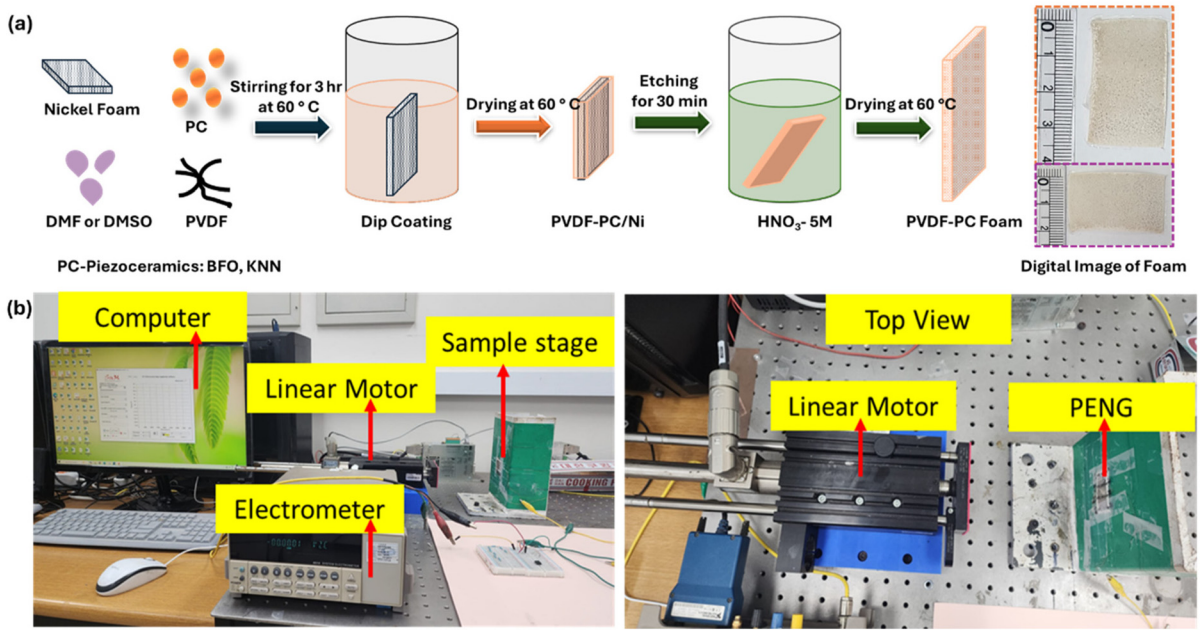

Fig. 1 (a) Schematic illustration of the fabrication process of the PVDF-piezoceramic composite foam and (b) digital images of the energy harvesting set-up, including a linear motor, an electrometer and the software interface of the control system.

PVDF-BFO) with chromium/gold as top and bottom electrodes deposited *via* magnetron sputtering (current: 20 mA; time: 120 s; temperature: RT; gas: argon) followed by encapsulating with antistatic tape to avoid any contact resistance or external disturbance. The copper wires were connected to both sides of the electrodes for measurement. Before electrical measurements, the devices were poled at 5 kV for 30 min *via* an electrode poling set-up. The open-circuit voltage and short-circuit current were measured at various load resistances (1 MΩ to 1.1 GΩ) using an Electrometer 6514 with force applied *via* a linear motor. The applied compressive force was roughly 2 N, with a moving mass of about 2 kg and an operating acceleration of 1 m s^{-2}.

3 Results and discussion

3.1 Physicochemical characterization

The XRD patterns of the fabricated foams are shown in Fig. 2a and b. The major peak at ~20° corresponds to the (110) and (200) diffraction planes of the β phase. The peaks corresponding to BFO (Fig. 2a) and KNN (Fig. 2b) are represented as '#'. The characteristic diffraction planes corresponding to the synthesized BFO and KNN are clearly indexed in the figure confirming that they exhibit a rhombohedral distorted perovskite structure and a tetragonal perovskite structure, respectively. The observed diffraction peaks of the ceramic fillers were exactly matched with the JCPDS card no. 86-1518 and PDF no. 00-065-0276 for BFO and KNN, respectively. Furthermore, the calculated degree of crystallinity values for PVDF, PVDF-2% BFO, PVDF-4%BFO, PVDF-2%KNN, and PVDF-4%KNN electrodes were found to be approximately 79%, 81%, 83%, 82%, and 85%, respectively. These results indicate a gradual increase in crystallinity with increasing filler content, confirming the role of ceramic fillers as effective heterogeneous nucleating agents.

Fig. 3a and b depict the FTIR spectra of the various fabricated foams consisting of α and β-phases. The absorption peaks at 873 and 1166 cm^{-1} occur due to the presence of the β-phase. The peak at 871 cm^{-1} corresponds to the CF_2 stretching and CH_2 rocking vibrations whereas the peaks at 1070, 1165, and 1400 cm^{-1} are due to the CF_2 stretching, C–C skeleton, and CH_2 deformation generated by the rocking vibrations. The absorption bands at 840 cm^{-1} (CF_2 rocking) and 1400 cm^{-1} (CH_2 bending) are a characteristic of the β-phase whereas the band at 762 cm^{-1} (skeletal bending and CF_2 bending) corresponds to the α-phase, respectively. Furthermore, using Beer–Lambert's law, the β-phase fraction percentage ($F(\beta)$) was estimated. It was observed that the $F(\beta)$ value increased from 75.2% to 76.3% for PVDF-2%-BFO and PVDF-4%-BFO. Similarly, the value increased from 70.8% for PVDF-2%-KNN to 71.3% for PVDF-4%-KNN. Thus, an enhancement in the β-phase value with an increase in filler content confirms that the β-phase value improved after the addition of ceramic fillers in the foam. Although only a slight increase in the β-phase content is observed, the incorporation of a large amount of piezoelectric ceramic fillers significantly enhances the overall performance due to synergistic effects arising from improved crystallinity, efficient stress transfer, and strong interfacial interactions, rather than β-phase content alone.

FE-SEM analysis was used to observe the morphology of the developed foams. In Fig. S1a and b, the FE-SEM images of the synthesized BFO and KNN nanoparticles reveal an agglomer-

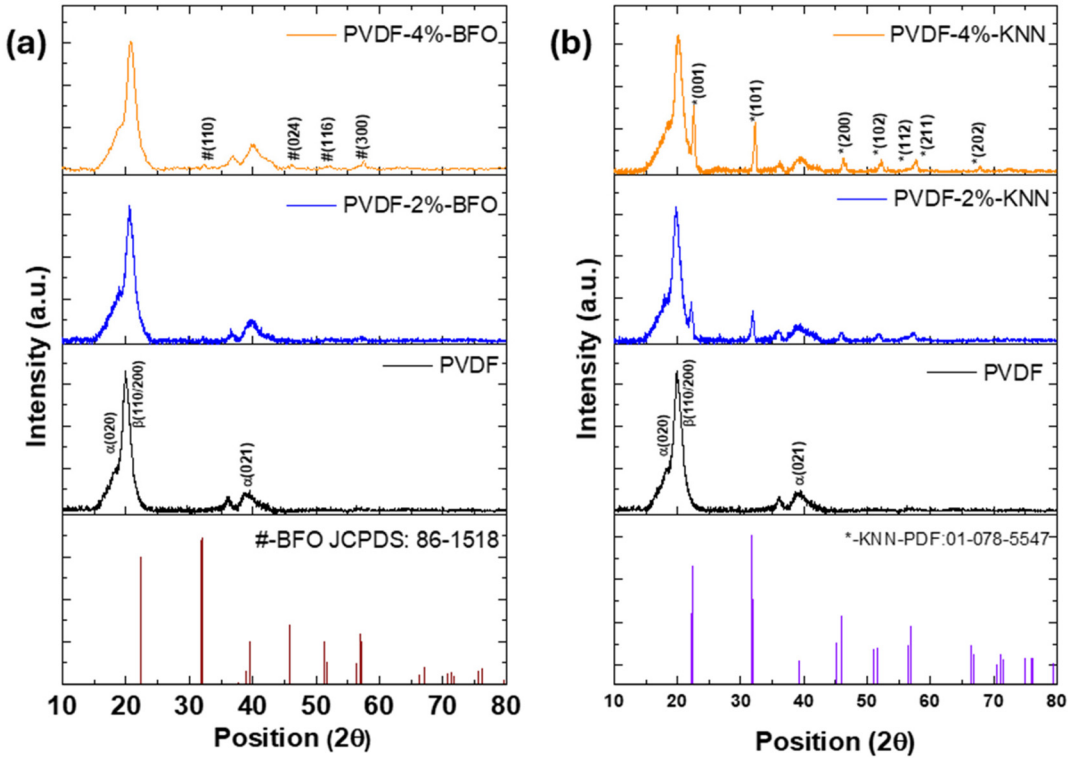

Fig. 2 XRD spectra of the (a) PVDF-BFO and (b) PVDF-KNN foams with pristine PVDF.

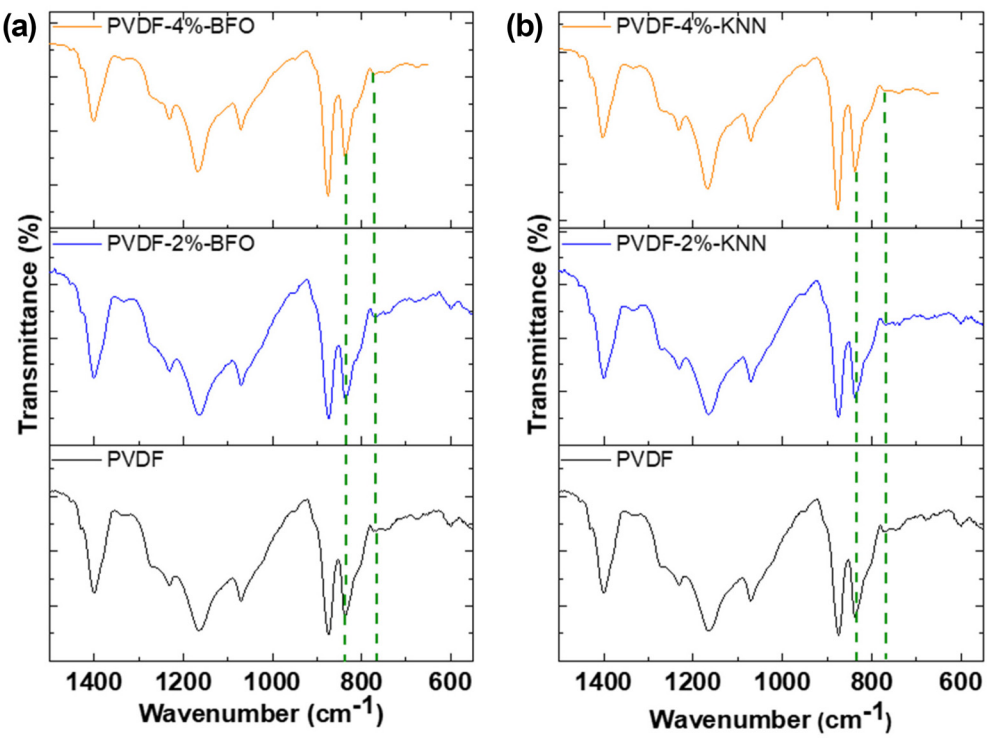

Fig. 3 FTIR spectra of the (a) PVDF-BFO and (b) PVDF-KNN foams with pristine PVDF.

ated structure with an average particle size of 300 nm and 500 nm, respectively. As inferred from the FE-SEM micrographs (Fig. 4), the fabricated polymer composite foams exhibit an honeycomb-like structure with many open gaps on the surface, with the NPs clearly embedded in the PVDF matrix (Fig. 4a–d), resulting in a well-integrated structure with an interconnected foam architecture and uniformly dispersed constituents. This confirms the existence of an open-cell, interconnected porous structure with continuous pore channels and no isolated voids. In line with the improved electromechanical response mentioned, this demonstrates the existence of a flexible and compressible network that promotes effective stress transfer. Crucially, all samples exhibit comparable microstructural characteristics within each composition, suggesting minimal batch-to-batch variance and adequate control over synthesis conditions. Therefore, the findings of the FE-SEM micrographs verify the development of a porous structure in the foam samples and the even dispersion of the NPs throughout the PVDF matrix.

Fig. 5a–d display the EDS spectra of the PVDF-2%-BFO, PVDF-4%-BFO, PVDF-2%-KNN, and PVDF-4%-KNN foams. The atomic percentages of the C, O, F, Bi, and Fe elements in the PVDF-2%-BFO foam (Fig. 5a) were 22.11, 18.71, 50.94, 4.88, and 3.36%, respectively. The C, O, F, Na, K, and Nb elements were detected in the PVDF-2%-KNN foam (Fig. 5c) with atomic percentages of 26.78, 18.23, 40.82, 7.51, and 6.46%, respectively. The elemental composition of the PVDF-4%-BFO (Fig. 5b) and PVDF-4%-KNN foams (Fig. 5d) was confirmed by EDS analysis as well. Furthermore, Fig. S2–S5 show the EDS mapping of PVDF-2%-BFO, PVDF-4%-BFO, PVDF-2%-KNN and PVDF-4%-KNN foams, where the presence of elements such as F, C, Bi, Fe and O for PVDF-BFO and F, C, K, Na, N, and O for PVDF-KNN confirm the uniform distribution of the piezoceramics (BFO and KNN) in the polymeric (PVDF) matrix. Their limited distribution is attributed to the low filler content (2% and 4%) compared to the polymer matrix (98% and 96%). Furthermore, no traceable amount of Ni was observed from the EDS analysis, which affirms the complete etching of Ni. Thus, the EDS results uncovered the existence of the fillers in the fabricated composite foams.

DSC analysis was performed to investigate the melting behaviour of the fabricated pristine and composite foam structures. Fig. S6 shows the DSC heating curves of the pristine PVDF and the composite foams with varying weight fractions of fillers. Fig. S6a indicates that the pure PVDF foam exhibits a melting temperature at about 161.5 °C and a small endothermic peak at a lower temperature (106 °C). The melting temperature of the α-phase PVDF is lower than that of the β-phase. This type of melting behavior arises due to double melting transitions very often observed in PVDF owing to its polymorphic structure. The first peak represents the melting of the α-phase, while the second peak at 161.5 °C is assigned to the

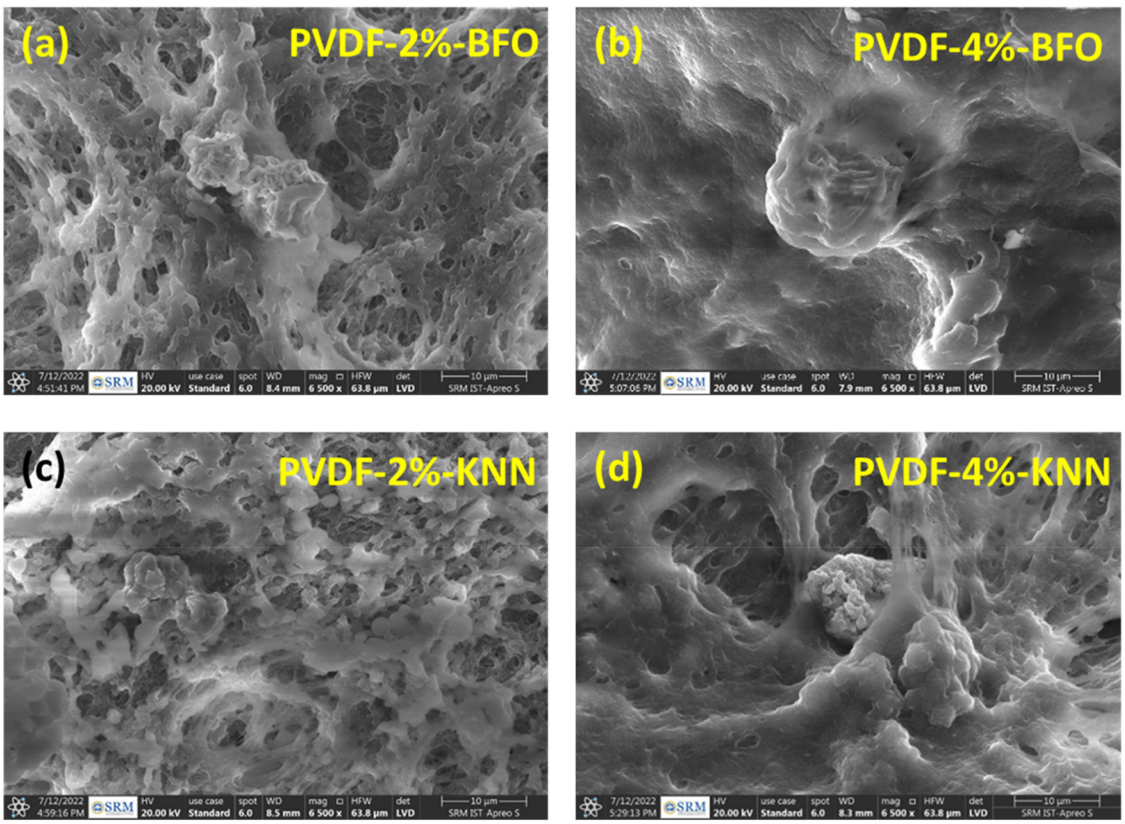

Fig. 4 FESEM micrographs of the composite foams (a) PVDF-2%-BFO, (b) PVDF-4%-BFO, (c) PVDF-2%-KNN, and (d) PVDF-4%-KNN.

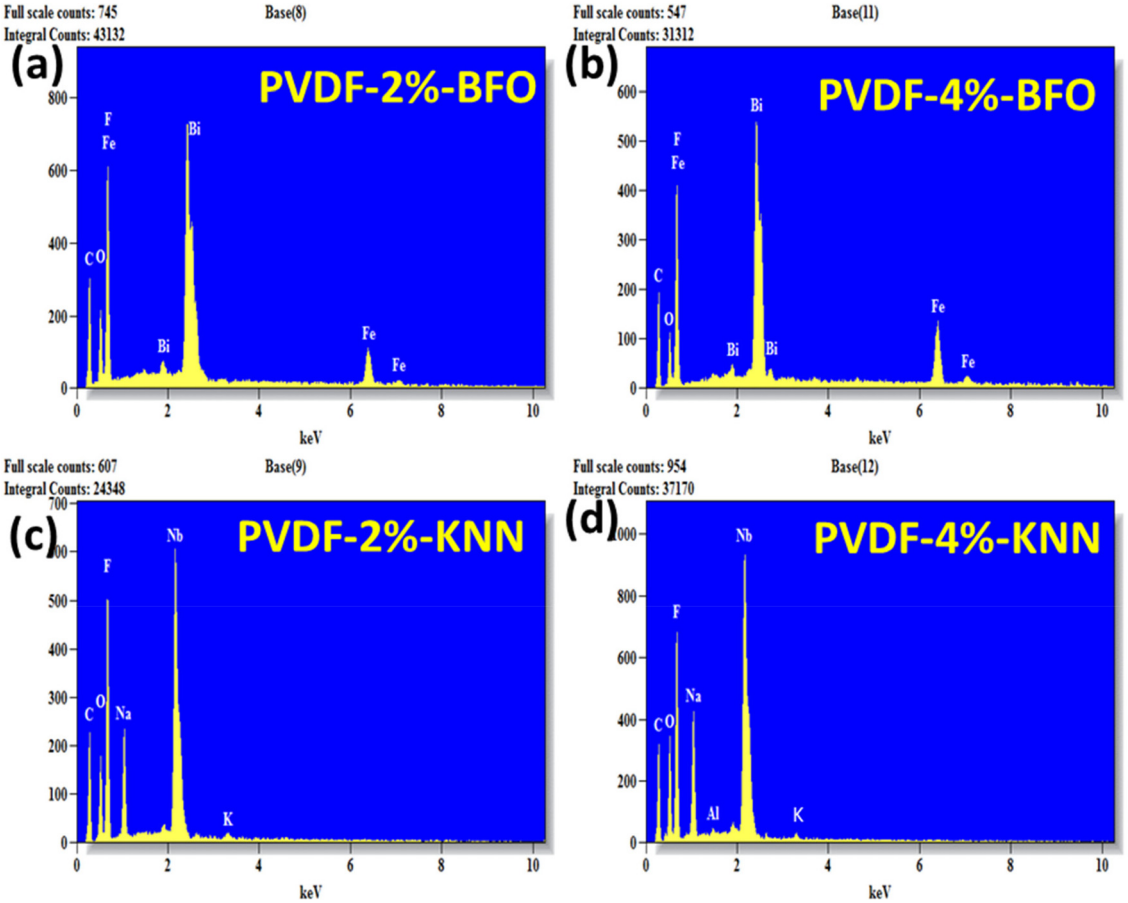

Fig. 5 EDS spectra of (a) PVDF-2%-BFO, (b) PVDF-4%-BFO, (c) PVDF-2%-KNN and (d) PVDF-4%-KNN foams.

β-phase of PVDF crystals. In the case of the composite foams, there is only one peak for each of the PVDF-BFO (Fig. S6a) and PVDF-KNN (Fig. S6b) foams. In the case of PVDF-BFO foams, the melting temperatures are 164.5 and 160.9 °C for composites containing 2 and 4 wt% BFO, respectively. Similarly, for PVDF-2%-KNN and PVDF-4%-KNN, the melting peaks are at 164.5 and 162.7 °C. It was observed that the melting point increased with the addition of 2 wt% filler in the PVDF composite foam. This feature can be attributed to the better dispersion of the NPs in the polymer matrix at a low filler

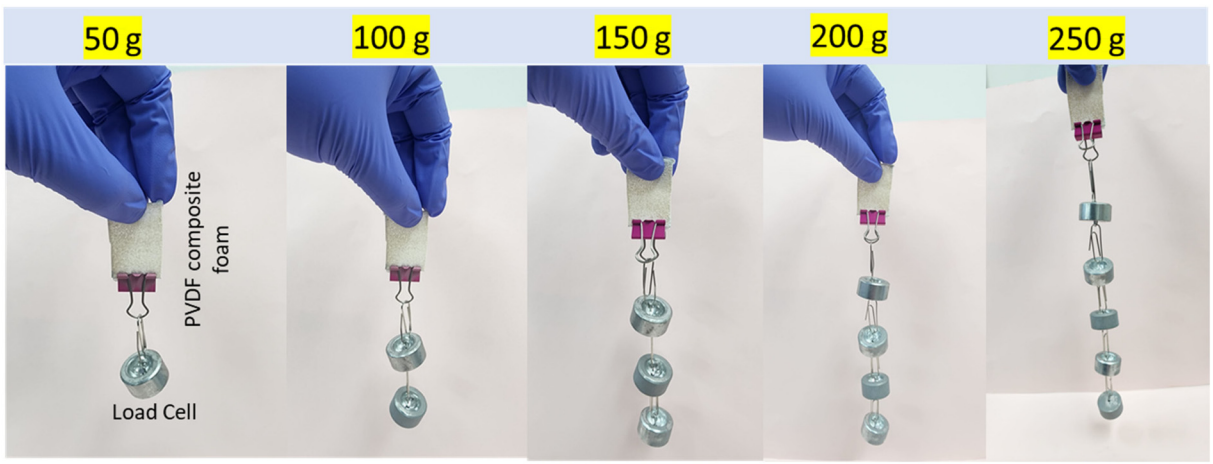

Fig. 6 Digital images of the load-bearing test of the PVDF composite foam.

loading, which promotes heterogeneous nucleation and facilitates the formation of more ordered crystalline domains. However, further increasing the filler loading to 4% leads to a decrease in the melting temperature, which may be due to the formation of imperfect crystalline domains that possess reduced lamellar thickness. The higher filler concentration induces interfacial constraints and limits polymer chain mobility, resulting in the formation of smaller and thermally less stable crystals. The TGA curves of the various foams are depicted in Fig. S6c and d. TGA analysis was performed to determine the thermal stability of the foams. It shows that the amount ultimately left over after foam degradation is higher for composite foams than for the virgin PVDF foam. Furthermore, it is evident that as the filler content increases, the weight percentage after degradation increases, supporting the proper loading of fillers into the composite foams matching the filler weight percentage.

The practical load-bearing and flexibility of the PVDF composite foam (PVDF-4%KNN) was assessed using a calibrated load cell, as shown in Fig. 6. The composite foam exhibited better structural integrity and elastic recovery, with no discernible deformation or fracture when loaded incrementally from

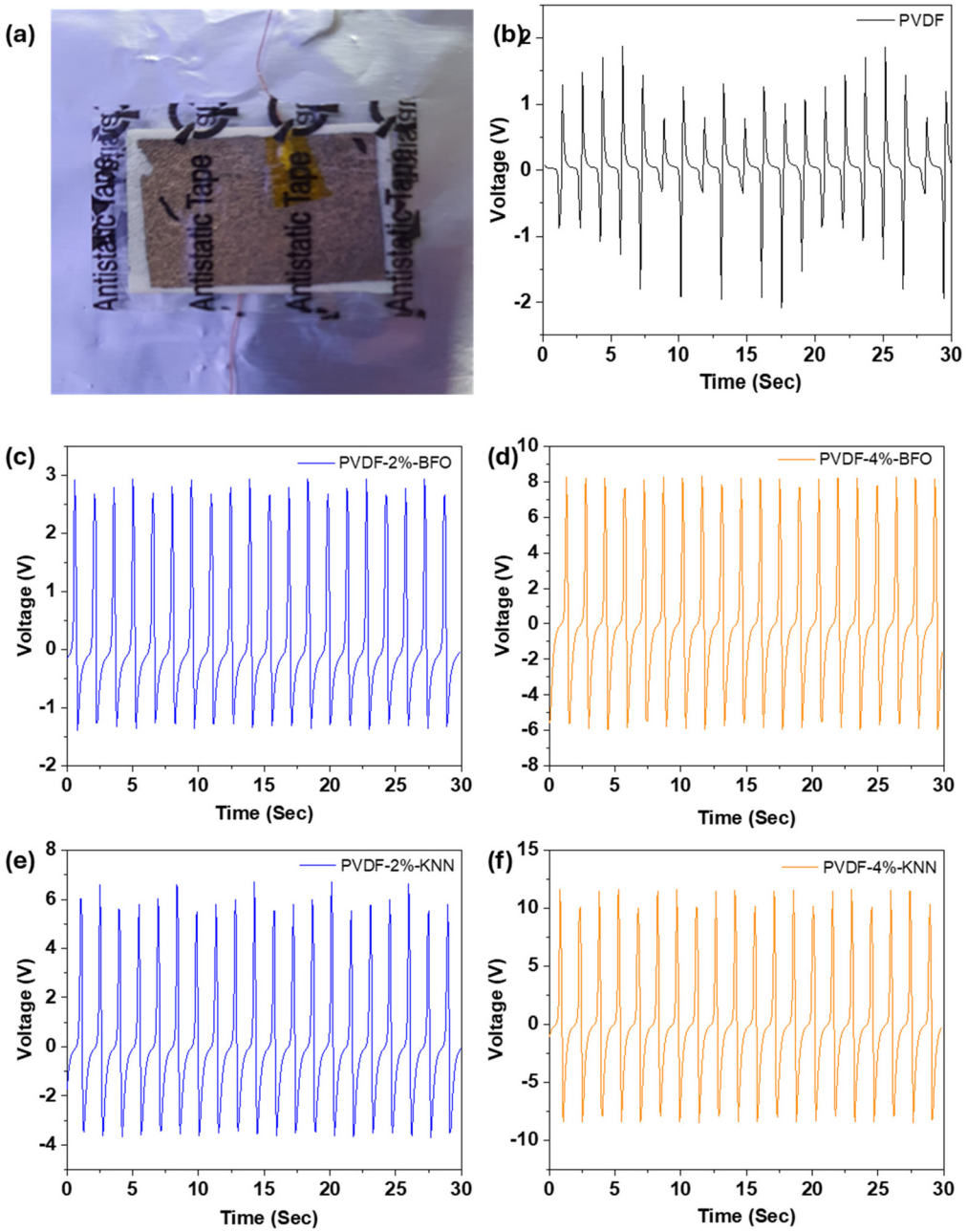

Fig. 7 (a) Digital image of the fabricated foam-based PENG device. Open circuit voltage of (b) PVDF, (c) PVDF-2%-BFO, (d) PVDF-4%-BFO, (e) PVDF-2%-KNN and (f) PVDF-4%-KNN foam-based PENG devices at 1 GΩ.

50 g to 250 g. This experiment confirms the material's suitability for wearable applications, where routine handling and moderate mechanical stresses are expected.

3.2 Piezoelectric property analysis

Fig. 7a depicts the digital image of the fabricated device. The poled composite foams were used to fabricate a PENG. The device was tested under the impact of a force generated by a linear motor. Mechanical energy that was applied to the nanogenerator was transformed into useable electrical energy that could be stored and used to power low-power devices later. The open-circuit voltage and short-circuit current, measured under the impact of a 1 m s^{-2} acceleration at various load resistances from 1 MΩ to 1.1 GΩ, are shown in Fig. S7a–d and S8a–d, respectively.

The output voltage and current (Fig. 7b and 8a) of the pristine PVDF foam are 2 V and 25 nA, respectively. As can be seen in Fig. 7c and d, the PVDF-2%-BFO foam gives an output

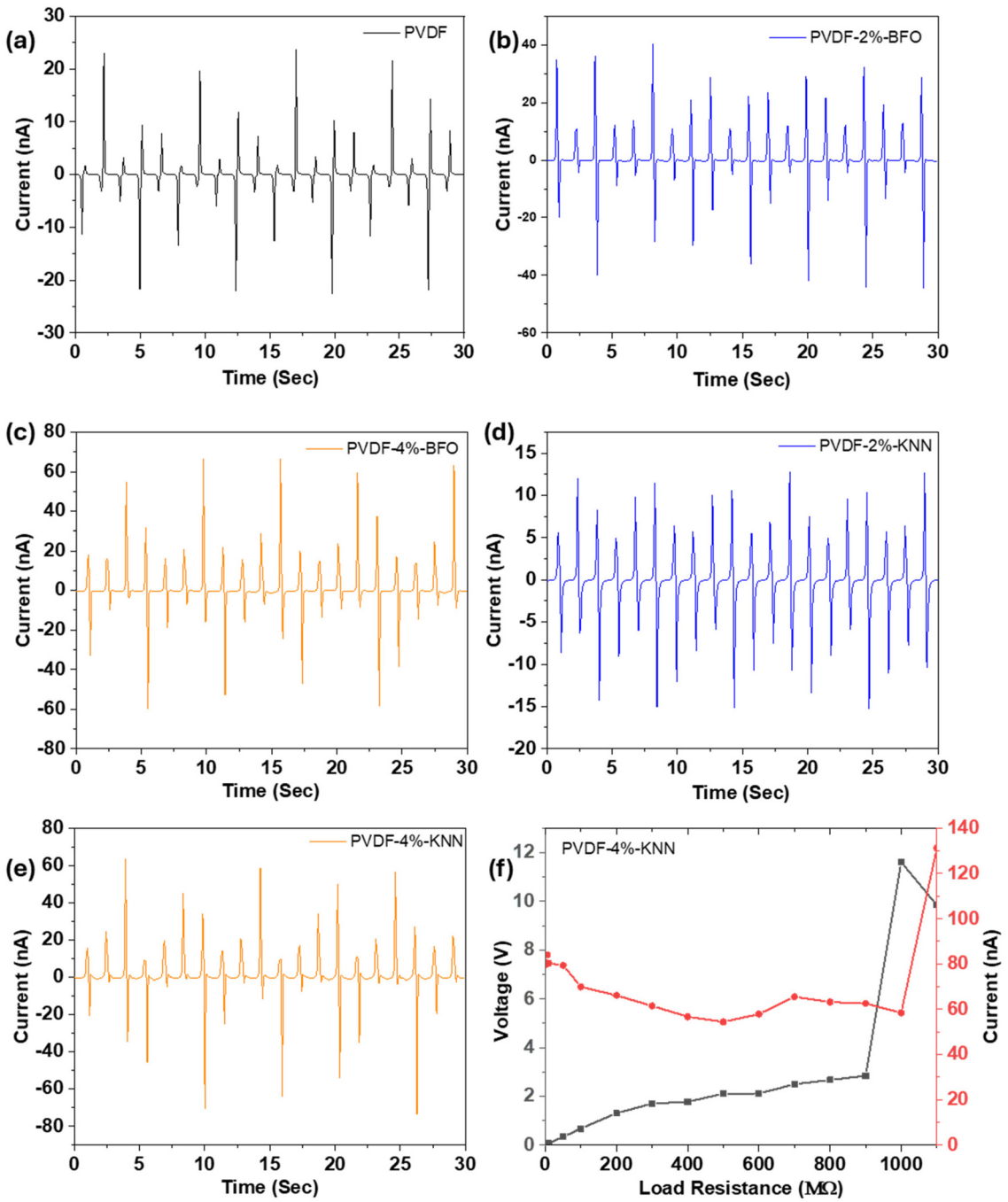

Fig. 8 Output current generated by the (a) PVDF, (b) PVDF-2%-BFO, (c) PVDF-4%-BFO, (d) PVDF-2%-KNN and (e) PVDF-4%-KNN foam-based PENG devices at 1 GΩ. (f) Open circuit voltage and short-circuit current of PVDF-4%-KNN foam-based PENG devices at various load resistances.

voltage of about 2.95 V whereas PVDF-4%-BFO generates a higher voltage of ~8.35 V. Similarly, in the case of PVDF-2%-KNN and PVDF-4%-KNN based PENGs, the output voltage increases with increased loading of KNN NPs in PVDF-2%-KNN and PVDF-4%-KNN delivering ~6.73 V and 11.61 V, respectively (Fig. 7e and f). Thus, for both types of foams, it is observed that the output voltage increases with increasing filler content. Also, the PVDF-4%-KNN foam-based PENG device produced the maximum output voltage of ~11.61 V at 1 GΩ load resistance, indicating that 1 GΩ is the matching load resistance for the device. Furthermore, Fig. 8 shows the current generated by the composite foams. PVDF-2%-BFO and PVDF-4%-BFO foam-based PENGs (Fig. 8b and c) deliver output currents of ~35 nA and 66 nA, respectively, whereas for the foams PVDF-2%-KNN and PVDF-4%-KNN (Fig. 8d and e), the values are ~13 nA and 70 nA, respectively. It is observed that the output voltage of the composite foam is higher (difference ~7.83 V and 25 nA) than that of the pristine foam, and also, the performance increases with increasing filler content. Moreover, it is observed that the PVDF-KNN foam-based PENGs deliver better output voltage than the PVDF-BFO-based PENGs, and the forward and reverse bias characteristics of the PVDF-4%-KNN device are shown in Fig. S9a and b. The output performances of the fabricated foam-based PENG devices were compared to those of the recently reported PVDF and its copo-

Table 1 Comparison of the current work with similar recent studies

PENG material	Output voltage (V)	Output current (nA)	Ref.
PVDF-MWCNT foam	12 V	30	40
PDMS-BTO-MWCNT foam	1.5 V	—	27
PVDF foam	7 V	75	41
PVDF/ZIF-8 foam	10 V	90	42
PVDF foam	4.1	70	43
Polypropylene foam	5.7	—	44
PVDF foam	4.7	43.6	45
PVDF foam	11.84	217.78	36
PVDF foam	19.1	580	46
PVDF-BT foam	12.5	150	39
PVDF foam	3.78	45	Present work
PVDF-BFO foam	~8.35	~66	Present work
PVDF-KNN foam	~11.61	~70	Present work

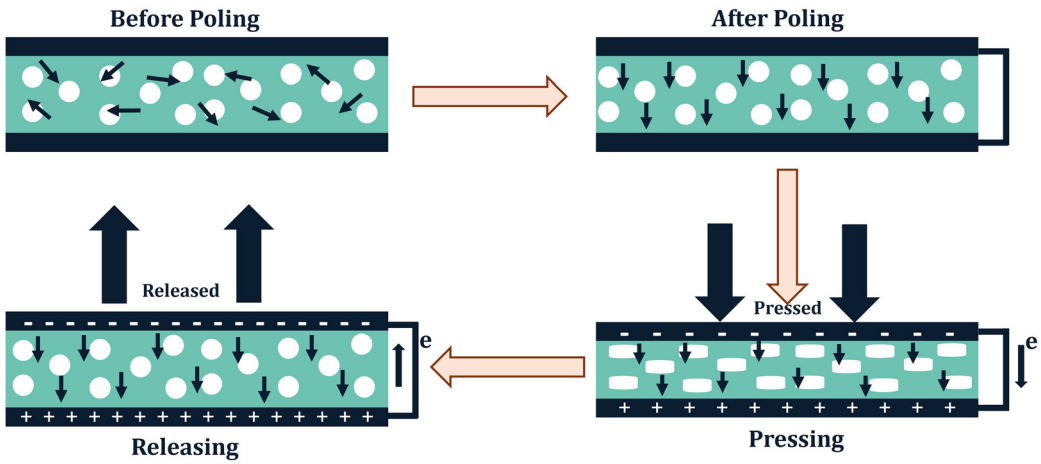

Fig. 9 Schematic diagram of the operating mechanism of the PENG.

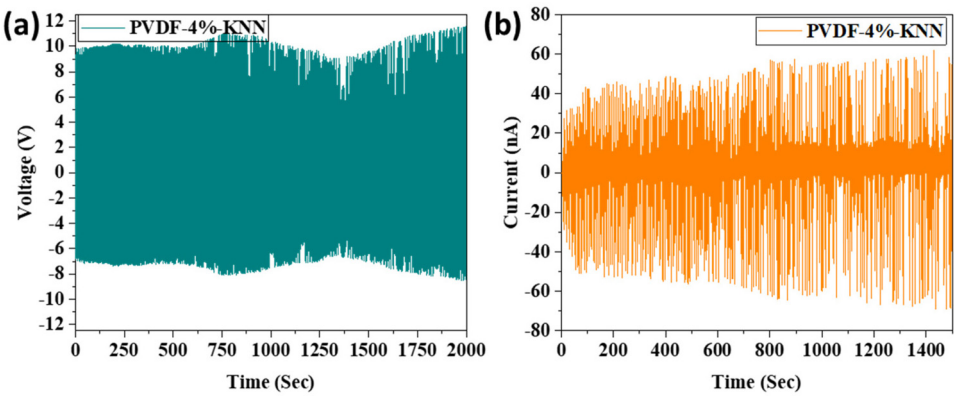

Fig. 10 Stability tests of PVDF-KNN devices: (a) output voltage and (b) current.

lymer-based composite nanogenerators (Table 1). It can be clearly observed that the filler content in the reported studies is higher than that used in the current work. Thus, the 3D porous foam structure offers a continuous pathway for easy transfer of load and hence results in better performance.

Fig. 9 depicts a schematic representation of the PENG's internal functioning mechanism: (i) The dipoles in the piezoceramic materials are initially arranged arbitrarily when no poling is present; (ii) when an electric field is applied to the device, the dipoles tend to align themselves in the direction of the field. When there is no impact from a human palm, there is no development of an electric signal, and it remains in a state of balance; (iii) the piezoelectric potential is created between the electrodes of the device as a result of the compressive strain that is caused by the application of a human palm impact to the device. An AC output signal is produced while this operation is being carried out; and (iv) finally, a tiny flexible force that emerges after releasing a palm hit produces a reverse piezoelectric potential.

Furthermore, the long-term stability of the PVDF-2%-BFO, PVDF-4%-BFO, PVDF-2%-KNN (Fig. S10a–c) and PVDF-4%-KNN (Fig. 10a and b) foam-based PENG devices for 600 seconds under the impact of an acceleration of 1 m s^{-2} was tested. It showed an almost constant peak-to-peak voltage throughout the 400 consecutive cycles, which indicates the better performance of the fabricated composite devices. In

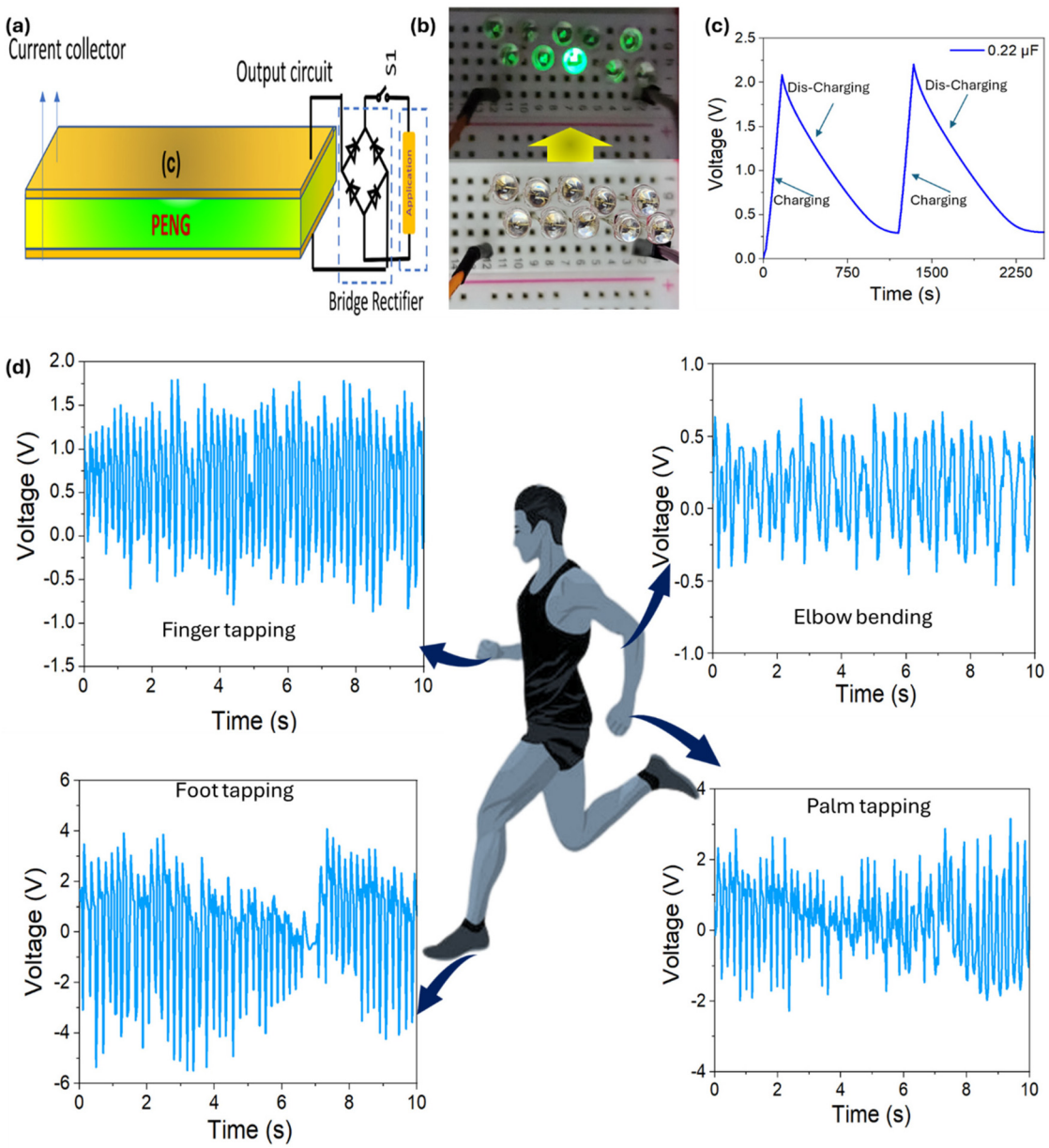

Fig. 11 (a) Rectifier circuit, (b) lighting up of the green LEDs, and (c) charging pattern of the capacitor *via* a foam-based PENG device. (d) Generating voltage under various biomechanical movements: finger tapping, elbow bending, foot tapping, and palm tapping.

addition, a commercial capacitor with a capacity of 0.22 μF was used to test the PENG's ability to charge capacitors. It is observed that the charging voltage increased at an exponential rate, reaching its maximum value of 2.0 V in approximately 165 seconds. This was done by charging the capacitor with the rectified output that was acquired from a bridge rectifier (Fig. 11a). The PENG was connected with green LEDs in the absence of any energy storage device in order to determine whether or not it would be useful for real-world applications. The PENG was able to instantaneously light up the green LEDs (Fig. 11b) whenever they were subjected to the impact of finger tapping. In addition, the charging pattern of the capacitor using the PENG is displayed in Fig. 11c, which depicts the pressing and releasing modes of operation. Furthermore, the feasibility of the as-fabricated PENG device as a biomechanical energy harvester was tested under different conditions (finger, foot, palm tapping, and elbow bending), by placing a device in the body (Fig. 11d). The foot tapping-based biomechanical energy exhibited higher output compared to other body motions. The applied force during various actuation modes was quantitatively measured using a pressure sensor, as shown in Fig. S11. The average forces recorded during finger, palm, and foot tapping were approximately 10 N, 20 N, and 35 N, respectively. The acquired results confirmed that the composite devices outperformed the pristine devices in terms of output. The results show that the output voltage increases as piezoceramic KNN content in the foam increases from 2 wt% to 4 wt%. These findings support the possible use of a foam-based PENG as a biomechanical energy harvester in various places, including toll booths, as well as for various motion sensors used in biomedical devices, traffic monitoring systems, tactile sensors, wireless sensors, *etc*.

4 Conclusion

In summary, a simple and scalable approach was used to create a flexible, lightweight, lead-free ceramic polymer composite foam. In this context, the piezoelectric foam was fabricated *via* molding a sacrificial nickel framework with PVDF-ceramic NPs (BFO and KNN) dispersed, followed by etching of the Ni template. The composite-based PVDF-KNN device exhibited greater piezoelectric output voltage and current of 11.61 V and 70 nA when compared to the pristine PVDF foam. The foam devices also demonstrated good stability, which engenders their used in a variety of applications. Despite the low filler weight fraction, the PENG demonstrates better performance compared to conventional composite films, owing to its 3D interconnected architecture, which facilitates continuous load transfer, which is difficult to achieve in low-filler conventional composites. Thus this work presents a scalable method for farbicating a ceramic–polymer composite based on an interconnected 3D piezoelectric foam structure, highlighting a novel material platform for self-powered micromechanical devices and efficient energy harvesting applications.

Conflicts of interest

The authors declare having no known competing financial interest or personal relationship that could influence the work reported in this paper.

Data availability

The data supporting this article have been included as part of the supplementary information (SI). Supplementary information: synthesis of BFO and KNN nanoparticles, characterization methods, FESEM of BFO and KNN nanoparticles, EDS mapping, and PENG evaluation of the prepared PVDF and PVDF composite foam devices. See DOI: https://doi.org/10.1039/d6lp00034g.

Acknowledgements

The authors acknowledge the funding from the Department of Science and Technology (Ref. SP/YO/2019/1432), Government of India, New Delhi, for the research work.

References

1 S. Park, H. Kim, M. Vosgueritchian, S. Cheon, H. Kim, J. H. Koo, T. R. Kim, S. Lee, G. Schwartz, H. Chang and Z. Bao, Stretchable Energy-Harvesting Tactile Electronic Skin Capable of Differentiating Multiple Mechanical Stimuli Modes, *Adv. Mater.*, 2014, **26**, 7324–7332.
2 F. R. Fan, W. Tang and Z. L. Wang, Flexible Nanogenerators for Energy Harvesting and Self-Powered Electronics, *Adv. Mater.*, 2016, **28**, 4283–4305.
3 H. Wu, Y. Huang, F. Xu, Y. Duan and Z. Yin, Energy Harvesters for Wearable and Stretchable Electronics: From Flexibility to Stretchability, *Adv. Mater.*, 2016, **28**, 9881–9919.
4 Z. Chen, H. Yang, H. Yu, T. Yu, L. Liu, Y. Lu and W. Gao, PVDF/PANi@HNT Nanocomposite Membranes: Pioneering Solutions for Piezoelectric Sensing and Energy Harvesting Efficiency, *ACS Appl. Mater. Interfaces*, 2025, **17**, 28668–28681.
5 D. K. Bharti, S. Kumar and J. P. Singh, High-performance, temperature retardant and hydrophobic $BiCoO_3$:PDMS piezoelectric nanogenerator for effective energy harvesting in harsh environments, *Chem. Eng. J.*, 2026, **532**, 174311.
6 J. Zou, Z. Jiang, J. Kim, C. Wu and J. Park, Performance Enhancement of $BaTiO_3$-PDMS Flexible Piezoelectric Nanogenerator using Double ZTO Microsphere monolayers, *Ceram. Int.*, 2026, DOI: 10.1016/j.ceramint.2026.04.034.
7 K. Shi, Y. Zhang, S. Taleb, H. Phillips-Brene, E. Wilhelm and M. Acuautla, Boosted Output of Flexible PANI@BTO/PVDF–TrFE Piezoelectric Nanogenerators for Self-powered Multifunctional Sensing in Wearable Systems, *Chem. Eng. J.*, 2026, **535**, 175420.

8 K. Kukreja, S. Pratihar, P. K. Panda and P. K. S. Mural, High-performance Piezoelectric Nanogenerator based on PVDF/2D Layered Mo_3AlC_2 Composites for Sustainable Energy Harvesting Applications, *Sens. Actuators, A*, 2026, **399**, 117415.
9 J.-H. Lee, K. Y. Lee, M. K. Gupta, T. Y. Kim, D.-Y. Lee, J. Oh, C. Ryu, W. J. Yoo, C.-Y. Kang, S.-J. Yoon, J.-B. Yoo and S.-W. Kim, Highly Stretchable Piezoelectric-Pyroelectric Hybrid Nanogenerator, *Adv. Mater.*, 2014, **26**, 765–769.
10 L. Persano, C. Dagdeviren, Y. Su, Y. Zhang, S. Girardo, D. Pisignano, Y. Huang and J. A. Rogers, High Performance Piezoelectric Devices based on Aligned Arrays of Nanofibers of Poly(vinylidenefluoride-co-trifluoroethylene), *Nat. Commun.*, 2013, **4**, 1633.
11 Z. Zhang, C. Yao, Y. Yu, Z. Hong, M. Zhi and X. Wang, Mesoporous Piezoelectric Polymer Composite Films with Tunable Mechanical Modulus for Harvesting Energy from Liquid Pressure Fluctuation, *Adv. Funct. Mater.*, 2016, **26**, 6760–6765.
12 C. Sun, J. Shi, D. J. Bayerl and X. Wang, PVDF Microbelts for Harvesting Energy from Respiration, *Energy Environ. Sci.*, 2011, **4**, 4508–4512.
13 D. Zabek, J. Taylor, E. L. Boulbar and C. R. Bowen, Micropatterning of Flexible and Free Standing Polyvinylidene Difluoride (PVDF) Films for Enhanced Pyroelectric Energy Transformation, *Adv. Energy Mater.*, 2015, **5**, 1401891.
14 S. Horiuchi and Y. Tokura, Organic ferroelectrics, *Nat. Mater.*, 2008, **7**, 357–366.
15 W. Zhang, Q. Feng, E. Hosono, D. Asakura, J. Miyawaki and Y. Harada, Tetragonal Distortion of a BaTiO3/Bi0.5Na0.5TiO3 Nanocomposite Responsible for Anomalous Piezoelectric and Ferroelectric Behaviors, *ACS Omega*, 2020, **5**, 22800–22807.
16 C.-T. Pan, S.-Y. Wang, C.-K. Yen, A. Kumar, S.-W. Kuo, J.-L. Zheng, Z.-H. Wen, R. Singh, S. P. Singh, M. T. Khan, R. K. Chaudhary, X. Dai, A. Chandra Kaushik, D.-Q. Wei, Y.-L. Shiue and W.-H. Chang, Polyvinylidene Fluoride-Added Ceramic Powder Composite Near-Field Electrospinned Piezoelectric Fiber-Based Low-Frequency Dynamic Sensors, *ACS Omega*, 2020, **5**, 17090–17101.
17 S. Song, Y. Li, Q. Wang and C. Zhang, Boosting Piezoelectric Performance with a New Selective Laser Sintering 3D Printable PVDF/graphene Nanocomposite, *Composites, Part A*, 2021, **147**, 106452.
18 Y. Xu, L. Jin, X. He, X. Huang, M. Xie, C. Wang, C. Zhang, W. Yang, F. Meng and J. Lu, Glowing Stereocomplex Biopolymers are Generating Power: Polylactide/carbon Quantum Dot Hybrid Nanofibers with High Piezoresponse and Multicolor Luminescence, *J. Mater. Chem. A*, 2019, **7**, 1810–1823.
19 Y. Mao, P. Zhao, G. McConohy, H. Yang, Y. Tong and X. Wang, Sponge-Like Piezoelectric Polymer Films for Scalable and Integratable Nanogenerators and Self-Powered Electronic Systems, *Adv. Energy Mater.*, 2014, **4**, 1301624.
20 Y. Zhang, C. R. Bowen and S. Deville, Ice-templated Poly(vinylidene fluoride) Ferroelectrets, *Soft Matter*, 2019, **15**, 825–832.
21 T. Kowalchik, F. Khan, K. Le, P. Leland, S. Roundy and R. Warren, Effect of Pore Structure on the Piezoelectric Properties of Barium Titanate-Polyvinylidene Fluoride Composite Films, *Nano Energy*, 2023, **109**, 108276.
22 M. Hassanpour Amiri and K. Asadi, How Porosity Affects the Performance of Piezoelectric Energy Harvesters and Sensors, *Adv. Phys. Res.*, 2023, **2**, 2200042.
23 K. Okazaki and K. Nagata, Effects of Grain Size and Porosity on Electrical and Optical Properties of PLZT Ceramics, *J. Am. Ceram. Soc.*, 1973, **56**, 82–86.
24 K. Ina, T. Mano and S. O. Nagata, Hydrophone Sensitivity of Porous Pb(Zr, Ti)O_3 Ceramics, *Jpn. J. Appl. Phys.*, 1994, **33**, 5381.
25 Y.-C. Chen and S. Wu, Piezoelectric composites with 3–3 connectivity by injecting polymer for hydrostatic sensors, *Ceram. Int.*, 2004, **30**, 69–74.
26 C. N. Della and D. Shu, The performance of 1–3 piezoelectric composites with a porous non-piezoelectric matrix, *Acta Mater.*, 2008, **56**, 754–761.
27 W. R. McCall, K. Kim, C. Heath, G. La Pierre and D. J. Sirbuly, Piezoelectric Nanoparticle–Polymer Composite Foams, *ACS Appl. Mater. Interfaces*, 2014, **6**, 19504–19509.
28 B. A. Tuttle, J. E. Smay, J. Cesarano, J. A. Voigt, T. W. Scofield, W. R. Olson and J. A. Lewis, Robocast Pb$(Zr_{0.95}Ti_{0.05})O_3$ Ceramic Monoliths and Composites, *J. Am. Ceram. Soc.*, 2001, **84**, 872–874.
29 M. Allahverdi, S. C. Danforth, M. Jafari and A. Safari, Processing of Advanced Electroceramic Components by Fused Deposition Technique, *J. Eur. Ceram. Soc.*, 2001, **21**, 1485–1490.
30 K. Boumchedda, M. Hamadi and G. Fantozzi, Properties of a hydrophone produced with porous PZT ceramic, *J. Eur. Ceram. Soc.*, 2007, **27**, 4169–4171.
31 H. Kara, R. Ramesh, R. Stevens and C. R. Bowen, Porous PZT Ceramics for Receiving Transducers, *IEEE Trans. Ultrason. Ferroelectr. Freq. Control*, 2003, **50**, 289–296.
32 V. Wilkens and W. Molkenstruck, Broadband PVDF Membrane Hydrophone for Comparisons of Hydrophone Calibration Methods up to 140 MHz, *IEEE Trans. Ultrason. Ferroelectr. Freq. Control*, 2007, **54**, 1784–1791.
33 M. Toda and J. Dahl, PVDF Corrugated Transducer for Ultrasonic Ranging Sensor, *Sens. Actuators, A*, 2007, **134**, 427–435.
34 S. J. Kang, Y. J. Park, I. Bae, K. J. Kim, H.-C. Kim, S. Bauer, E. L. Thomas and C. Park, Printable Ferroelectric PVDF/PMMA Blend Films with Ultralow Roughness for Low Voltage Non-Volatile Polymer Memory, *Adv. Funct. Mater.*, 2009, **19**, 2812–2818.
35 F. Wang, M. Tanaka and S. Chonan, Development of a PVDF Piezopolymer Sensor for Unconstrained In-Sleep Cardiorespiratory Monitoring, *J. Intell. Mater. Syst. Struct.*, 2003, **14**, 185–190.

36 L. Song, Z. Huang, S. Guo, Y. Li and Q. Wang, Hierarchically Architected Polyvinylidene Fluoride Piezoelectric Foam for Boosted Mechanical Energy Harvesting and Self-Powered Sensor, *ACS Appl. Mater. Interfaces*, 2021, **13**, 37252–37261.

37 H.-Q. Liang, Q.-Y. Wu, L.-S. Wan, X.-J. Huang and Z.-K. Xu, Thermally Induced Phase Separation Followed by In situ Sol–gel Process: A Novel Method for PVDF/SiO_2 Hybrid Membranes, *J. Membr. Sci.*, 2014, **465**, 56–67.

38 L. Song, R. Dai, Y. Li, Q. Wang and C. Zhang, Polyvinylidene Fluoride Energy Harvester with Boosting Piezoelectric Performance through 3D Printed Biomimetic Bone Structures, *ACS Sustainable Chem. Eng.*, 2021, **9**, 7561–7568.

39 J. Guo, Q. Wu, C. Zhang, Y. Li, M. Nie, Q. Wang and Y. Liu, Porosity Manipulation to Boost Piezoelectric Output via Supercritical Carbon Dioxide Foaming and Surface Modification, *Mater. Des.*, 2022, **217**, 110616.

40 S. Badatya, D. K. Bharti, N. Sathish, A. K. Srivastava and M. K. Gupta, Humidity Sustainable Hydrophobic Poly(vinylidene fluoride)-Carbon Nanotubes Foam Based Piezoelectric Nanogenerator, *ACS Appl. Mater. Interfaces*, 2021, **13**, 27245–27254.

41 Y. Zhao, S. Shi, Z. Ma, G. Li and X. Liao, Polymorphism Regulation in Poly(vinylidene fluoride) Foam Achieved by Supercritical CO_2 Foaming Assisted with Ionic Liquid for High-Performance Piezoelectric Device, *Compos. Sci. Technol.*, 2025, **261**, 111031.

42 J. Chen, L. Song, F. Qi, S. Qin, X. Yang, W. Xie, K. Gai, Y. Han, X. Zhang, Z. Zhu, H. Cai, X. Pei, Q. Wan, N. Chen, J. Wang, Q. Wang and Y. Li, Enhanced Bone Regeneration via ZIF-8 Decorated Hierarchical Polyvinylidene Fluoride Piezoelectric Foam Nanogenerator: Coupling of Bioelectricity, Angiogenesis, and Osteogenesis, *Nano Energy*, 2023, **106**, 108076.

43 Y. Zhao, B. Wang, S. Zeng, S. Shi, G. Li and X. Liao, β-phase Formation of Poly(vinylidene fluoride) Foam based on the Porous Morphology Control via Supercritical Carbon Dioxide, *Sustainable Mater. Technol.*, 2024, **40**, e00987.

44 C. Ravikumar and V. Markevicius, Ferroelectret Polypropylene Foam-Based Piezoelectric Energy Harvester for Different Seismic Mass Conditions, *Actuators*, 2023, **12**, 215.

45 X. Chen, T. Ding, X. Wu, M. Qin, Q. Cai, H. Tai and Q. Li, Enhanced Piezoelectric Output Performance in Flexible Polyvinylidene Fluoride Foam with a Hierarchical Dual-pore Structure, *J. Mater. Chem. C*, 2025, **13**, 13529–13541.

46 X. Liu, X. Li, X. Wei, J. Chen, Y. Li and C. Zhang, Supercritical Fluid Foaming of Self-Polarized β-PVDF Piezoelectric Foam with Tailored Cells for Advanced Energy Harvesting, *ACS Appl. Mater. Interfaces*, 2025, **17**, 40499–40507.